# α2-Chimaerin is essential for neural stem cell homeostasis in mouse adult neurogenesis

Yi-Ting Su[a], Shun-Fat Lau[a], Jacque P. K. Ip[a], Kit Cheung[a], Tom H. T. Cheung[a], Amy K. Y. Fu[a,b], and Nancy Y. Ip[a,b,1]

[a]Division of Life Science, Molecular Neuroscience Center, State Key Laboratory of Molecular Neuroscience, The Hong Kong University of Science and Technology, Clear Water Bay, Hong Kong, China; and [b]Guangdong Provincial Key Laboratory of Brain Science, Disease and Drug Development, The Hong Kong University of Science and Technology Research Institute, Shenzhen, 518057 Guangdong, China

Adult hippocampal neurogenesis involves the lifelong generation of neurons. The process depends on the homeostasis of the production of neurons and maintenance of the adult neural stem cell (NSC) pool. Here, we report that α2-chimaerin, a Rho GTPase-activating protein, is essential for NSC homeostasis in adult hippocampal neurogenesis. Conditional deletion of α2-chimaerin in adult NSCs resulted in the premature differentiation of NSCs into intermediate progenitor cells (IPCs), which ultimately depleted the NSC pool and impaired neuron generation. Single-cell RNA sequencing and pseudotime analyses revealed that α2-chimaerin–conditional knockout (α2-CKO) mice lacked a unique NSC subpopulation, termed Klotho-expressing NSCs, during the transition of NSCs to IPCs. Furthermore, α2-CKO led to defects in hippocampal synaptic plasticity and anxiety/depression-like behaviors in mice. Our findings collectively demonstrate that α2-chimaerin plays an essential role in adult hippocampal NSC homeostasis to maintain proper brain function.

chimaerin | Rho GTPase | adult neurogenesis | neural stem cells | neural progenitors

Adult neurogenesis in the mammalian hippocampus involves the lifelong generation of neurons, which integrate into preexisting neuronal network (1, 2). Impaired neurogenesis is associated with cognitive impairment and psychiatric diseases, including major depression. Neural stem cells (NSCs) in the subgranular zone (SGZ) of the dentate gyrus (DG) in the adult hippocampus, also named radial glia-like cells (RGLs), give rise to excitatory granule neurons through a precise program of cellular proliferation and differentiation. First, a quiescent NSC becomes activated and gives rise to one NSC and one neuronal progenitor cell (NPC)/intermediate progenitor cell (IPC); the latter proliferates and subsequently differentiates into a fate-determined neuroblast (NB) or astroglia (1). Finally, the NB matures into an excitatory granule neuron, which integrates into the molecular layer to modulate cognitive functions and mood regulation (3).

Activation of quiescent NSCs prepares them for differentiation into IPCs during adult neurogenesis. Maintaining and replenishing the NSC pool is critical for ensuring that sufficient neurons are generated and that the NSC pool is not prematurely depleted (1, 4). Prolonged NSC quiescence or failure to activate can hamper the replenishment of the active NSC pool, leading to compromised regenerative ability (5, 6). Alternatively, premature differentiation of NSCs depletes the NSC pool, gradually decreasing neurogenesis and ultimately impairing normal brain functions such as cognition and emotion control (7, 8). Recent single-cell RNA sequencing (scRNA-seq) studies demonstrate that the NSC pool is a heterogeneous amalgamation of distinct cell populations, covering the spectrum from quiescence to activation, each with unique neurogenic potential (9–11).

Recent studies suggest that both extrinsic and intrinsic signals regulate NSC self-maintenance and differentiation under a highly sophisticated microenvironment, which constantly determines whether NSCs undergo quiescence, activation, or terminal differentiation. Extrinsically, the neurogenic niche, which

includes blood vessels, endothelial cells, astrocytes, microglia, and mature neurons, is thought to house the NSCs and orchestrate their proper transition from self-renewal to differentiation (12, 13). For example, NSCs are found anatomically close to the vasculature, enabling direct access to circulation-derived cytokines and growth factors that support their quiescence or activation status (14, 15). On the other hand, intrinsic factors including the transcriptional regulators, epigenetic modifiers, signaling pathways, and cytoskeletal organizers also orchestrate the fate of NSCs (16, 17). For instance, given that NSC activation is characterized by a transition of metabolic activity from glycolysis to oxidative phosphorylation, pathways that regulate cellular metabolic programs, such as nutrient-sensing signaling pathways (e.g., insulin-like growth factor I [IGF-I] signaling and PI3K/AKT/mTOR signaling), have been suggested to be signaling hubs that dictate NSC quiescence, activation, and differentiation processes (18). Thus, identifying the molecular mechanism(s) that governs the behaviors of NSCs would help to understand how this development program is coordinated.

Rho GTPases, a superfamily of small guanine nucleotide-binding proteins, are essential messengers that receive extracellular signals and translate extrinsic signals into intracellular events. This family of GTPases are under the spatiotemporal

**Significance**

Adult hippocampal neurogenesis, the lifelong generation of neurons in the dentate gyrus, is important for brain functioning, including learning, memory, and mood regulation. Its dysregulation is associated with cognitive decline and mood disorders. We discovered that the Rho GTPase-activating protein, α2-chimaerin, is essential for adult hippocampal neurogenesis, as it precisely regulates the transition of neural stem cells (NSCs) into intermediate progenitor cells (IPCs). Conditional knockout of α2-chimaerin in adult NSCs in the mouse hippocampus resulted in a loss of the Klotho-expressing NSC population and the premature differentiation of NSCs into IPCs, which impaired neuron production. These mice also exhibited compromised hippocampal synaptic plasticity and anxiety/depression-like behaviors. Thus, our findings revealed that α2-chimaerin is important in adult hippocampal neurogenesis.

control of their corresponding guanine nucleotide exchange factors (GEFs), GTPase-activating proteins (GAPs), and guanine nucleotide dissociation inhibitors (GDIs). Accordingly, Rho GTPases such as RhoA, Rac1, and Cdc42 regulate actin or microtubule assembly, modulate cell asymmetry by directly interacting with polarity proteins, or activate transcriptional factors to induce global changes in transcriptional profiles (19–21). It is well established that Rho GTPases actively modulate a plethora of processes in the adult hippocampus, including cellular proliferation and differentiation, dendritic development, and spine maturation (21–24). However, how the regulatory proteins of Rho GTPases are involved in adult hippocampal neurogenesis is largely unexplored.

In the present study, we showed that α2-chimaerin, a Rho GTPase-activating protein (RhoGAP), is essential for adult NSC homeostasis and regulates the neuronal lineage progression. By combining lineage tracing and scRNA-seq analysis, we showed that conditional knockout of α2-chimaerin in adult hippocampal NSCs led to premature differentiation of NSCs, which resulted in the absence of a unique NSC subpopulation: Klotho-expressing NSCs ($Kl^+$ NSCs). In the long term, this exhausted the NSC pool and decreased final neuron production. In addition, α2-CKO mice exhibited decreased dendritic growth in adult-born neurons, impaired synaptic plasticity, and deficits in anxiety/depression-like behaviors. Therefore, our results suggest that α2-chimaerin serves critical roles in the molecular regulation of NSC transition in adult neurogenesis to maintain proper brain function.

## Results

### Knockout of α2-Chimaerin Results in Decreased Proliferation of Adult NSCs/NPCs.
As a first step to examine the roles of α2-chimaerin in the adult hippocampus, we showed that α2-chimaerin protein was expressed in the granular layer and adjacent SGZ of the DG in the adult mouse hippocampus, where NSCs reside (*SI Appendix*, Fig. S1*A*). Specifically, α2-chimaerin was found in the proliferating, Nestin-expressing adult NSCs/NPCs (*SI Appendix*, Fig. S1 *B* and *C*). To examine whether α2-chimaerin regulates adult hippocampal neurogenesis, we labeled the proliferative cells in the DG in homozygous α2-chimaerin–germline knockout mice (α2-KO mice) by pulse injections of BrdU (5-bromo-2′-deoxyuridine) and performed immunostaining for Ki67, a cell cycling marker. Compared with the wild-type mice (WT mice), we observed fewer proliferating cells in the SGZ in the α2-KO mice (Ki67$^+$ cells: 43% fewer, BrdU$^+$ cells: 34% fewer; Fig. 1 *A*–*C*). In addition, the cultured adult NSCs/NPCs derived from the SGZ of α2-KO mice had a lower incorporation rate of EdU (5-ethynyl-2′-deoxyuridine) (39% lower; Fig. 1 *D* and *E*). These results further indicate that α2-chimaerin deletion leads to impaired proliferation of NSCs/NPCs. In the α2-KO mice, the DG volume remained relatively unchanged (*SI Appendix*, Fig. S1 *D* and *E*) and there was no abnormal apoptosis (Fig. 1 *F* and *G* and *SI Appendix*, Fig. S1*F*) or abnormal cell cycle exit events (Fig. 1 *H*–*J*). Cell proliferation in the subventricular zone of the α2-KO mice was similar to that in the WT mice (*SI Appendix*, Fig. S1 *G*–*I*). Therefore, these results collectively suggest that α2-chimaerin regulates NSC/NPC proliferation primarily in the adult mouse hippocampus.

Among the proliferating cells, compared with the WT mice, the percentage of Nestin$^+$BrdU$^+$ NSCs was significantly lower (by 27%) in the DG in the α2-KO mice, whereas the percentage of Tbr2$^+$BrdU$^+$ IPCs increased concomitantly (by 17%). Meanwhile, the percentage of DCX$^+$BrdU$^+$ NBs remained comparable between the WT and α2-KO mice (*SI Appendix*, Fig. S1 *J* and *K*). Thus, our results suggest that loss of α2-chimaerin results in the premature differentiation of NSCs into IPCs in the adult hippocampus, without affecting the fate determination of NSCs.

### Inducible, Conditional Knockout of α2-Chimaerin in Adult NSCs Causes the Premature Differentiation of NSCs/NPCs.
To investigate the direct role of α2-chimaerin in adult hippocampal NSCs, we conditionally deleted α2-chimaerin in Nestin-positive adult NSCs by injection of tamoxifen (TAM) at different time points (Fig. 2*A* and *SI Appendix, Methods*). There was no significant difference in the number of YFP$^+$ cells in the DG between the α2-chimaerin–conditional knockout mice (α2-CKO mice; Nes$^{CreERT2/+}$::R26R$^{YFP/+}$::α2-chimaerin$^{loxP/loxP}$) and control mice (CTRL mice; Nes$^{CreERT2/+}$::R26R$^{YFP/+}$::α2-chimaerin$^{+/+}$; *SI Appendix*, Fig. S2 *A* and *B*). This indicates that recombination efficiency was similar in both groups.

Next, we examined whether and how α2-chimaerin deletion in adult hippocampal NSCs regulates adult neurogenesis. Fate-mapping analysis revealed that the percentages of GFAP$^+$YFP$^+$ and Nestin$^+$YFP$^+$ NSCs in the SGZ were significantly lower in the α2-CKO mice than the CTRL mice at the initial stage 1 d after the last TAM injection (i.e., 1 d postinjection [dpi]) (GFAP$^+$YFP$^+$ cells: 29% lower, Nestin$^+$YFP$^+$ cells: 25% lower; Fig. 2 *B* and *D*). Furthermore, we observed a similar decrease in Nestin$^+$YFP$^+$ NSCs (by 21%) concomitant with an increase (by 120%) in the percentage of Tbr2$^+$YFP$^+$ IPCs in the α2-CKO DG at 10 dpi (Fig. 2 *C* and *E*); at this point, the Nestin$^+$ NSCs were differentiating into Tbr2$^+$ IPCs. Nonetheless, α2-chimaerin deletion in adult hippocampal NSCs did not affect the final differentiation of NSCs/NPCs: the percentage of DCX$^+$ NBs (DCX$^+$YFP$^+$ cells) remained relatively unchanged in the α2-CKO mice (Fig. 2*E*). Hence, our findings collectively suggest that loss of α2-chimaerin in adult NSCs leads to their premature differentiation into IPCs.

The premature differentiation of NSCs might lead to their differentiation into IPCs at the expense of self-renewal, resulting in the exhaustion of the NSC pool. Therefore, we examined whether the premature differentiation of NSCs perturbs the maintenance of the NSC pool and reduces neurogenesis in the α2-CKO mice in the long term. Indeed, the percentage of Nestin-expressing NSCs decreased further (57% lower) in the α2-CKO mice at 30 dpi (Fig. 2 *F* and *H*), demonstrating that α2-chimaerin deletion depletes the NSC pool. Concomitantly, compared with the CTRL mice, the α2-CKO mice exhibited reduced proliferation of NSCs/NPCs, as indicated by a lower percentage of BrdU$^+$YFP$^+$ dividing cells among YFP$^+$ cells (44% lower; Fig. 2*H* and *SI Appendix*, Fig. S2*C*). We then performed a long-term fate mapping experiment, which revealed a decrease in NeuN$^+$YFP$^+$ neurons at 90 dpi (by 23%; Fig. 2 *G* and *I*), whereas the number of neurons was unchanged at 30 dpi (Fig. 2*I* and *SI Appendix*, Fig. S2*D*). Thus, our results collectively suggest that the deletion of α2-chimaerin in adult hippocampal NSCs leads to the premature differentiation of NSCs into IPCs, which consequently depletes the NSC pool and decreases adult hippocampal neurogenesis in the long term.

### Regulation of Hippocampal NSC Subpopulations in the Adult DG Niche by α2-Chimaerin.
Our fate-mapping analysis indicated that α2-chimaerin might regulate adult hippocampal neurogenesis at different stages, i.e., the maintenance, proliferation, or differentiation of NSCs/NPCs. Given the complex and heterogeneous composition of NSCs/NPCs in the adult hippocampus, we performed scRNA-seq to compare the molecular identities of the NSC/NPC subpopulations and their distributions in the DG in adult α2-CKO mice and CTRL mice. We used fluorescence-activated cell sorting (FACS) to isolate all living cells from their DG niche after TAM injection and subjected them to droplet-based scRNA-seq (10× Genomics Chromium; see *SI Appendix*, *Methods*) (Fig. 3*A*). The final dataset retained 3,609 and 5,645 cells from the CTRL and α2-CKO mice, respectively. Then, we used *t*-distributed stochastic neighbor embedding (*t*-SNE) to separate the dataset, without bias, into separate cell clusters for
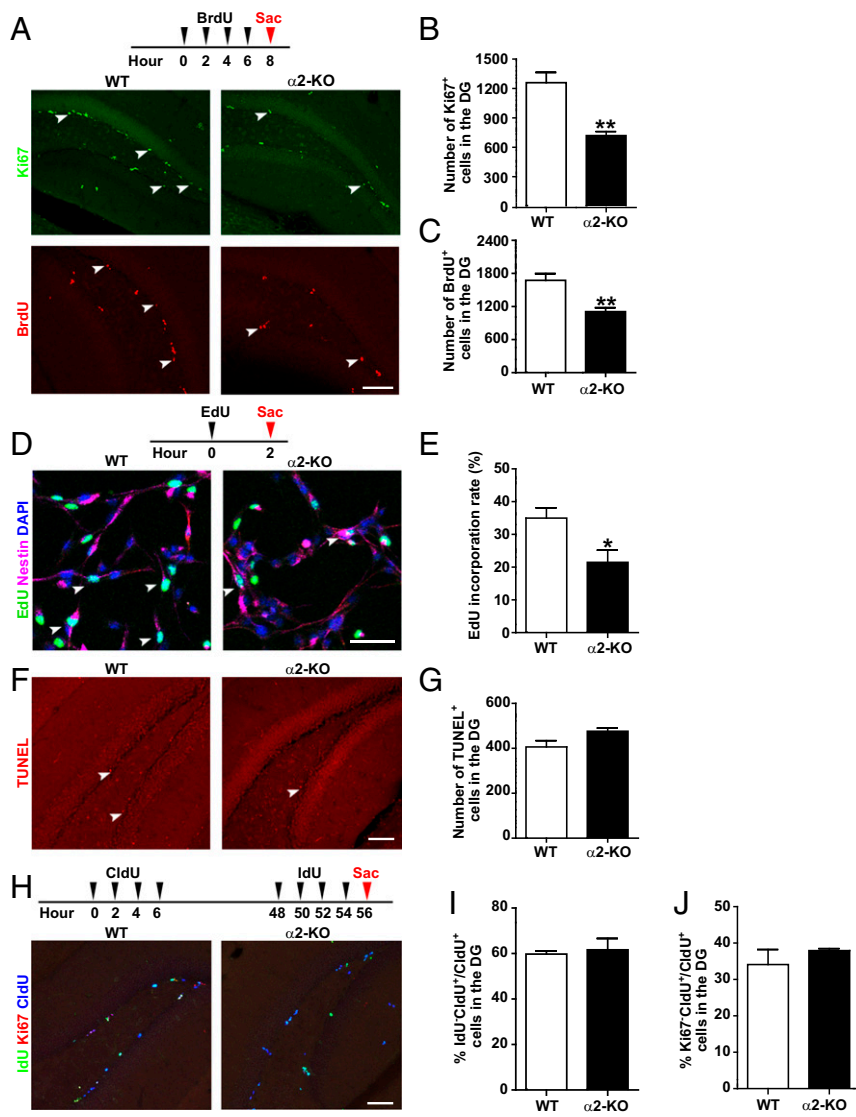
**Fig. 1.** Knockout of α2-chimaerin results in decreased proliferation of adult NSCs/NPCs. (*A*–*C*) Ki67 and BrdU labeling of NSCs/NPCs in the DG in WT and α2-KO mice on postnatal day 90. (*A*) Experimental paradigm (*Upper*), representative images (*Lower*), and quantification of Ki67$^+$ cells (*B*) and BrdU$^+$ cells (*C*) in the DG in WT and α2-KO mice. Arrowheads indicate labeled cells. Values are mean ± SEM ($n = 6$ per group; **$P < 0.01$; unpaired two-tailed $t$ test). (Scale bar: 75 μm.) (*D* and *E*) EdU labeling of proliferating cultured adult NSCs/NPCs from WT and α2-KO mice. (*D*) Experimental paradigm (*Upper*), representative images (*Lower*), and quantification (*E*) of EdU$^+$ proliferating cells from the cultured adult NSCs/NPCs derived from the SGZ of WT and α2-KO mice. Cell nuclei were labeled with DAPI. Arrowheads indicate labeled EdU$^+$Nestin$^+$ cells. Values are mean ± SEM ($n = 4$ independent batches; *$P < 0.05$; unpaired two-tailed $t$ test). (Scale bar: 50 μm.) (*F* and *G*) Labeling of apoptotic cells in the DG in WT and α2-KO mice. Representative images (*F*) and quantification (*G*) of TUNEL$^+$ cells in the DG in WT and α2-KO mice. Arrowheads indicate TUNEL$^+$ cells. Values are mean ± SEM ($n = 3$ per group; $P = 0.0890$; unpaired two-tailed $t$ test). (Scale bar: 75 μm.) (*H*–*J*) Labeling of cell cycle exit events in the DG in WT and α2-KO mice. (*H*) Experimental paradigm (*Upper*) and confocal images (*Lower*) of the DG from WT and α2-KO mice coimmunostained with IdU (5-iodo-2′-deoxyuridine), Ki67, and CldU (5-chloro-2′-deoxyuridine). Ki67$^-$CldU$^+$ or IdU$^-$CldU$^+$ cells represent cells that have exited the cell cycle by the time of CldU injection. (*I* and *J*) Quantification of the proportion of dividing cells in the DG in WT and α2-KO mice that exited the cell cycle after 48 h of sequential labeling. Values are mean ± SEM ($n = 3$ per group; Ki67$^-$CldU$^+$/CldU$^+$: $P = 0.4087$; IdU$^-$CldU$^+$/CldU$^+$: $P = 0.7426$; unpaired two-tailed $t$ test). (Scale bar: 75 μm.)

both groups (Fig. 3*B*). We then classified the major cell clusters on the basis of the expression of the significantly enriched and well-characterized marker genes within each cluster. The results showed that the cell clusters included NSCs (expressing *Clu*, *Aldoc*, *Id3*, and *Fabp7*), IPCs and NBs (expressing *Sox11*, *Neurod1*, *Dcx*, and *Eomes*), neurons (expressing *Snhg11*, *Ndnf*, and *Syt1*), oligodendrocytes (expressing *Mbp*, *Mog*, and *Olig1*), T cells (expressing *Cd3d* and *Cd3e*), and microglia (expressing *Csf1r*, *Cx3cr1*, and *Aif1*) (Fig. 3 *C* and *D*), which is consistent with the literature (9, 10, 25).

We subsequently identified five cell subpopulations of neuronal lineage from the *t*-SNE plot (Fig. 4*A*). Other than the IPCs/NBs and neurons (Fig. 3 *C* and *D*), three cell subpopulations expressed NSC markers, including *Clu*, *Aldoc*, *Id3*, and *Fabp7* (9, 10, 25) (Fig. 3*C*); among them, two subpopulations had similar transcriptome profiles (*SI Appendix*, Fig. S3*A*) that shared expression of *Aldoc* (*Aldoc*$^+$ NSCs hereafter; Fig. 4*B* and *SI Appendix*, Fig. S3*A*). Meanwhile, the remaining subpopulation did not express *Aldoc* but exclusively expressed *Kl*, which encodes an antiaging protein, Klotho (26, 27) (*Kl*$^+$ NSCs hereafter; Fig. 4*B* and *SI Appendix*, Fig. S3*A*). We then compared the distributions of cell populations of neuronal lineage between the CTRL and α2-CKO mice. Intriguingly, while the percentages of *Aldoc*$^+$ NSCs, IPCs/NBs, and neurons were comparable between

the CTRL and α2-CKO mice, *Kl*$^+$ NSCs were absent from the α2-CKO mice (Fig. 4 *A*–*C*).

**Kl-Expressing NSCs Represent a Transitional Stage Between *Aldoc*-Expressing NSCs and IPCs.** To determine the stage of adult neurogenesis in which *Kl*$^+$ NSCs are involved, we identified the molecular signature of *Kl*$^+$ NSCs by comparing the transcriptome profile of *Kl*$^+$ NSCs with those of *Aldoc*$^+$ NSCs, IPCs/NBs, and neurons. We identified 7,295 differentially expressed genes among these four subpopulations and performed K-means clustering analysis to further set these genes into six groups designated G1–G6 (*SI Appendix*, Fig. S3*B*). Among the six groups, G2 showed a gradient expression pattern ranging from *Aldoc*$^+$ NSCs and *Kl*$^+$ NSCs to IPCs/NBs and neurons. The expression levels of the top 20 differentially expressed genes in G2 were ordered, and various pan-NSC markers (i.e., *Dbi*, *Mt3*, *Clu*, *Id3*, and *Crip2*) (11, 28–30) decreased gradually in NSCs upon differentiation; the highest expression was observed in *Aldoc*$^+$ NSCs, followed by *Kl*$^+$ NSCs, IPCs/NBs, and finally neurons (Fig. 4*D*). Notably, *Kl*$^+$ NSCs had the highest expression of *Hmgn3* and *Suclg1* (Fig. 4*D*), which are important for neuronal progenitor differentiation (30, 31).

To understand the characteristics of this unique *Kl*$^+$ NSC population, we conducted gene ontology (GO) analysis, STRING
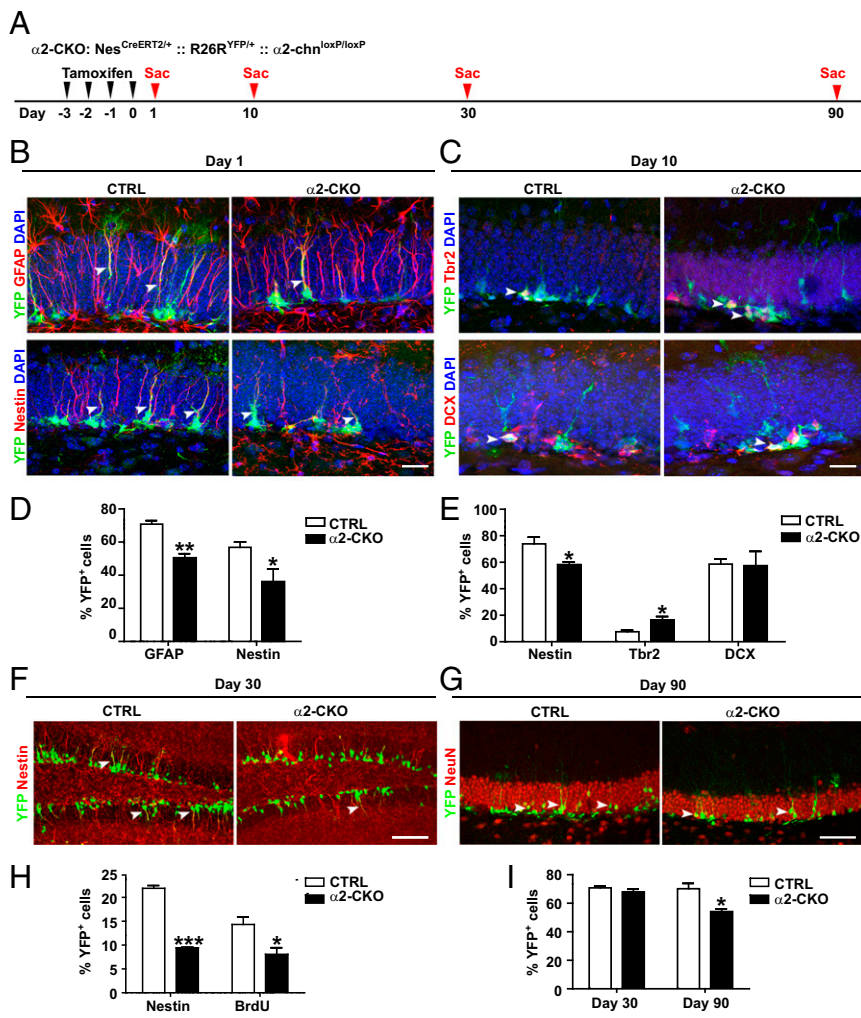
NEUROSCIENCE

**Fig. 2.** Conditional knockout of α2-chimaerin in adult NSCs leads to the premature differentiation of NSCs. (*A*) Schematic diagram of TAM administration to CTRL (Nes$^{CreERT2/+}$::R26R$^{YFP/+}$::α2-chimaerin$^{+/+}$) and α2-CKO (Nes$^{CreERT2/+}$::R26R$^{YFP/+}$::α2-chimaerin$^{loxP/loxP}$) mice on postnatal day 60. Following TAM injection, we collected the brains of the mice at 1, 10, 30, or 90 dpi. (*B*–*E*) NSCs differentiated prematurely in α2-CKO mice. Confocal images (*B*) and quantification (*D*) of the percentages of GFAP$^+$YFP$^+$ and Nestin$^+$YFP$^+$ cells (for NSCs) among YFP$^+$ cells in the DG in CTRL and α2-CKO mice at 1 dpi. Confocal images (*C*) and quantification (*E*) of the percentages of Nestin$^+$YFP$^+$, Tbr2$^+$YFP$^+$ cells (for IPCs) and DCX$^+$YFP$^+$ cells (for NBs) among YFP$^+$ cells in the DG in CTRL and α2-CKO mice at 10 dpi. Arrowheads indicate cells colabeled with YFP and specific cell-type markers. Values are mean ± SEM (1 dpi: GFAP$^+$YFP$^+$: $n = 3$ per group; **$P < 0.01$; Nestin$^+$YFP$^+$: $n = 4$ per group; *$P < 0.05$; 10 dpi: $n = 3$ per group; Nestin$^+$YFP$^+$: *$P < 0.05$; Tbr2$^+$YFP$^+$: *$P < 0.05$; DCX$^+$YFP$^+$: $P = 0.9266$; unpaired two-tailed $t$ test). (Scale bar: 25 μm.) (*F*–*I*) Lineage tracing of NSCs in the DG in CTRL and α2-CKO mice in the long term. Confocal images (*F*) and quantification (*H*) of the percentages of Nestin$^+$YFP$^+$ NSCs and BrdU$^+$YFP$^+$ proliferating NSCs/NPCs among YFP$^+$ cells in the DG in CTRL and α2-CKO mice at 30 dpi. Arrowheads indicate Nestin$^+$YFP$^+$ cells. Values are mean ± SEM ($n = 3$ per group; Nestin$^+$YFP$^+$: ***$P < 0.001$; BrdU$^+$YFP$^+$: *$P < 0.05$; unpaired two-tailed $t$ test). (Scale bar: 75 μm.) (*G* and *I*) Labeling of neurons generated in the DG in CTRL and α2-CKO mice in the long term. Confocal images (*G*) and quantification (*I*) of the percentage of NeuN$^+$YFP$^+$ mature neurons in the DG of CTRL and α2-CKO mice at 30 and 90 dpi. Arrowheads indicate the labeled NeuN$^+$YFP$^+$ cells. Values are mean ± SEM (30 dpi: CTRL: $n = 4$, α2-CKO: $n = 3$ per group; $P = 0.2356$; 90 dpi: $n = 3$ per group; *$P < 0.05$; unpaired two-tailed $t$ test). (Scale bar: 75 μm.)

analysis, and gene set enrichment analysis (GSEA) to compare the transcription profiles of $Kl^+$ NSCs. Both GO and STRING analysis showed that the top 100 significantly up-regulated genes in $Kl^+$ NSCs were related to biological processes and molecular functions associated with metabolic processes (i.e., electron transfer activity, ATP metabolic processes, and oxidative respiratory-related processes) compared with all other cell populations (GO) or to $Aldoc^+$ NSCs only (STRING) (Fig. 4*E* and *SI Appendix*, Fig. S3 *C* and *D*). In addition, GSEA comparing $Kl^+$ NSCs with $Aldoc^+$ NSCs revealed that a set of genes involved in Myc targets and PI3K_AKT_mTOR signaling as well as metabolic pathways in oxidative phosphorylation and fatty acid metabolism were highly expressed in $Kl^+$ NSCs (Fig. 4*F* and *SI Appendix*, Fig. S4*A*). Given that all of these pathways are involved in active metabolism and that a high metabolic status in NSCs can prime/promote the activation and differentiation of NSCs (32, 33), the results suggest that the $Kl^+$ NSCs might represent a subpopulation of NSCs that are prone to activation and differentiation to IPCs.

To determine whether $Kl^+$ NSCs represent a transition stage between $Aldoc^+$ NSCs and IPCs, we conducted a pseudotime trajectory analysis of all single cells by using a cluster-based, minimum spanning tree approach with tools for single cell analysis (TSCAN) to order the cells' progression on the basis of their transcriptome profile. Using the differentially enriched marker genes from each neuronal lineage cell types (Fig. 4*G*), TSCAN ordering recapitulated the expression dynamics of these genes during adult hippocampal neurogenesis. The results

showed that pan-NSC markers (i.e., *Aldoc*, *Clu*, *Id3*, and *Apoe*) decreased gradually along adult hippocampal neurogenesis. This further supports that $Kl^+$ NSCs represent a transition state between $Aldoc^+$ NSCs and IPCs along the following transition: $Aldoc^+$ NSCs → $Kl^+$ NSCs → IPCs/NBs → neurons (Fig. 4*H*). Thus, our results collectively suggest that $Kl^+$ NSCs represent a transition state NSCs between $Aldoc^+$ NSCs and IPCs.

**Conditional Knockout of α2-Chimaerin Leads to the Precocious Differentiation of NSCs and Alters Their Division Mode.** Regarding the molecular phenotypes of $Kl^+$ NSCs, the *t*-SNE plots showed that $Kl$ transcript was exclusively expressed in $Kl^+$ NSCs, whereas $Ttr$ transcript was expressed in different cell populations in the DG, with much higher expression in $Kl^+$ NSCs. Meanwhile, $Kl^+$ NSC was absent from the α2-CKO mice (i.e., $Kl^- Ttr^-$; Fig. 5 *A* and *B*). To examine the presence and spatial localization of $Kl^+$ NSCs in the mouse hippocampus, we conducted fluorescence in situ hybridization (FISH) and immunohistochemical analysis of the $Kl^+$ NSCs marker genes, $Kl$ and $Ttr$. Subset of cells in the SGZ of the DG in the CTRL mice highly expressed both $Kl$ and $Ttr$ transcripts, whereas similar cellular staining was not observed in the α2-CKO mice (Fig. 5 *C*–*E*). Specifically, Klotho and transthyretin (the protein encoded by $Ttr$ gene; Ttr hereafter) proteins were expressed in a subpopulation of Nestin-expressing YFP$^+$ NSCs in the DG in CTRL mice (*SI Appendix*, Fig. S5 *B* and *C*), confirming the presence of $Kl^+$ NSCs in the DG.

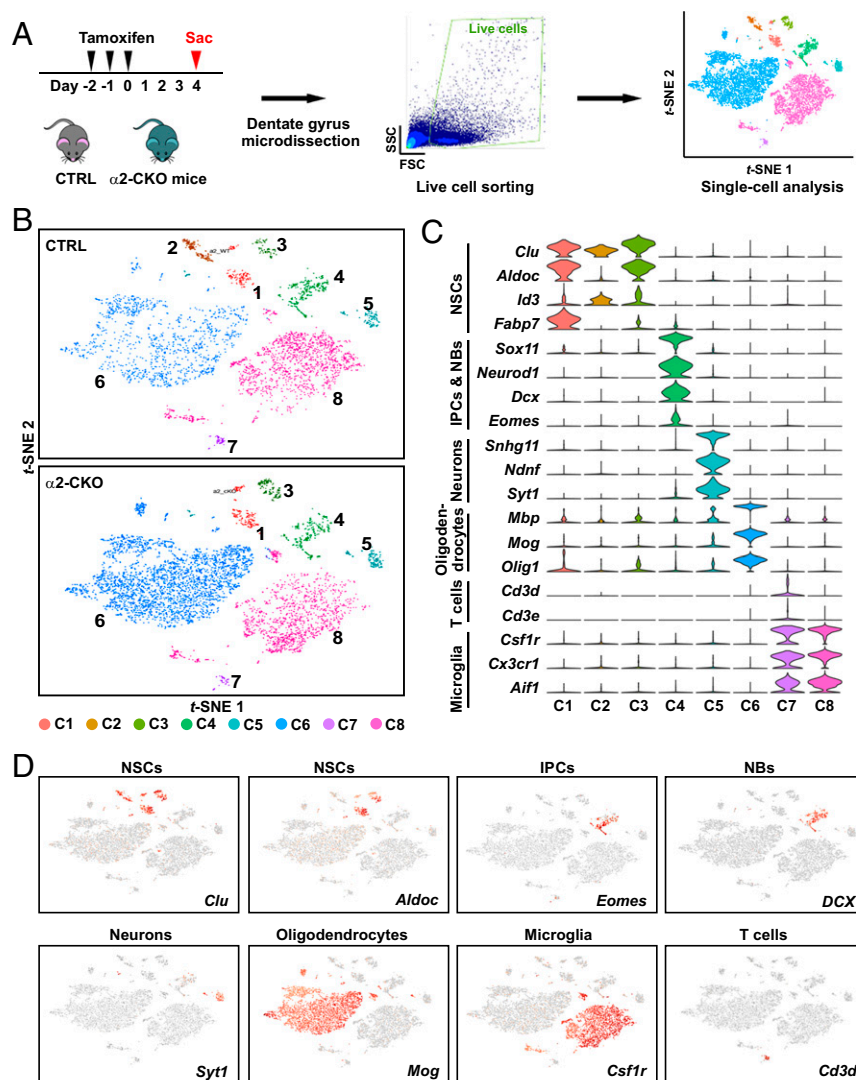**Fig. 3.** Cell-type analysis of the adult DG niche in CTRL and α2-CKO mice by single-cell RNA-seq. (*A*) Experimental strategy: CTRL and α2-CKO mice (*n* = 3 per group) received three TAM injections, and the DGs were isolated and microdissected at 4 dpi (*Left*). Single cells were purified by FACS (*Middle*), and the cells were then subjected to the 10× Genomics pipeline for single-cell RNA-seq (*Right*). (*B*) *t*-SNE maps show eight and seven cell clusters (C1–C8 and C1–C7) in the CTRL and α2-CKO mice, respectively. Each dot represents one cell, and each color represents one cell cluster. (*C*) Violin plots comparing the expressions of selected significant up-regulated cell-type marker genes in different cell clusters. The *y* axis indicates the normalized expression levels of the corresponding marker genes. (*D*) *t*-SNE maps showing the expressions of representative markers for each cell type. Cells are colored according to their expression levels, ranging from "not detected" (gray) to "highest detected" (red).

The loss of RNA transcript for the gene signature of $Kl^+$ NSCs in α2-CKO mice at 4 dpi (Fig. 5 *C–E* and *SI Appendix*, Fig. S5*A*) prompted us to lineage trace the fate of $Kl^+$ NSCs in the α2-CKO mice. We found that while 32% of NSCs in the DG in the CTRL mice were $Kl^+$ NSCs (i.e., Klotho$^+$YFP$^+$), this population decreased significantly in the α2-CKO mice at 1 dpi to 20% of the YFP$^+$ NSCs (Fig. 5 *F* and *G*). Importantly, the proportion of $Kl^+$ NSCs (i.e., Klotho$^+$YFP$^+$) dropped further to 6% in the α2-CKO mice at 4 dpi compared with 40% in the CTRL mice (Fig. 5*H*). We also observed a similar reduction of Ttr$^+$YFP$^+$ cells (for $Kl^+$ NSCs) at 1 dpi (*SI Appendix*, Fig. S5 *D* and *E*). Together, our findings suggest that conditional knockout of α2-chimaerin leads to the loss of the $Kl^+$ NSC subpopulation during adult neurogenesis.

The depletion of $Kl^+$ NSCs in the α2-CKO mice suggests that knockout of α2-chimaerin in NSCs might cause the precocious activation and differentiation of NSCs, which result in the depletion of the NSC pool. Indeed, we observed a significant increase (by 96%) in activated NSCs/NPCs labeled by

MCM2$^+$GFAP$^+$YFP$^+$ in the α2-CKO mice (Fig. 5 *I* and *J*), suggesting that the number of activated NSCs/NPCs increased in the hippocampus in the α2-CKO mice.

NSCs/NPCs undergo asymmetric division and give rise to one self-renewing radial glia-like NSC and another nonradial glia-like IPC; switching from asymmetric to self-depleting symmetric division results in the production of two IPCs and therefore a smaller NSC/NPC population (34). Importantly, most activated NSCs/NPCs (i.e., MCM2$^+$GFAP$^+$YFP$^+$) in the CTRL mice underwent asymmetric division as reported previously (34) (Fig. 5 *K* and *M*). Meanwhile, in the α2-CKO mice, these activated NSCs/NPCs exhibited an increased proportion of symmetric division, giving rise to two IPCs that exhibited neither a radial glial shape nor expressed the NSC marker, GFAP (Fig. 5 *K* and *M*). These findings suggest that the precocious differentiation of NSCs results in a switch of the division mode of NSCs/NPCs in the α2-CKO mice.

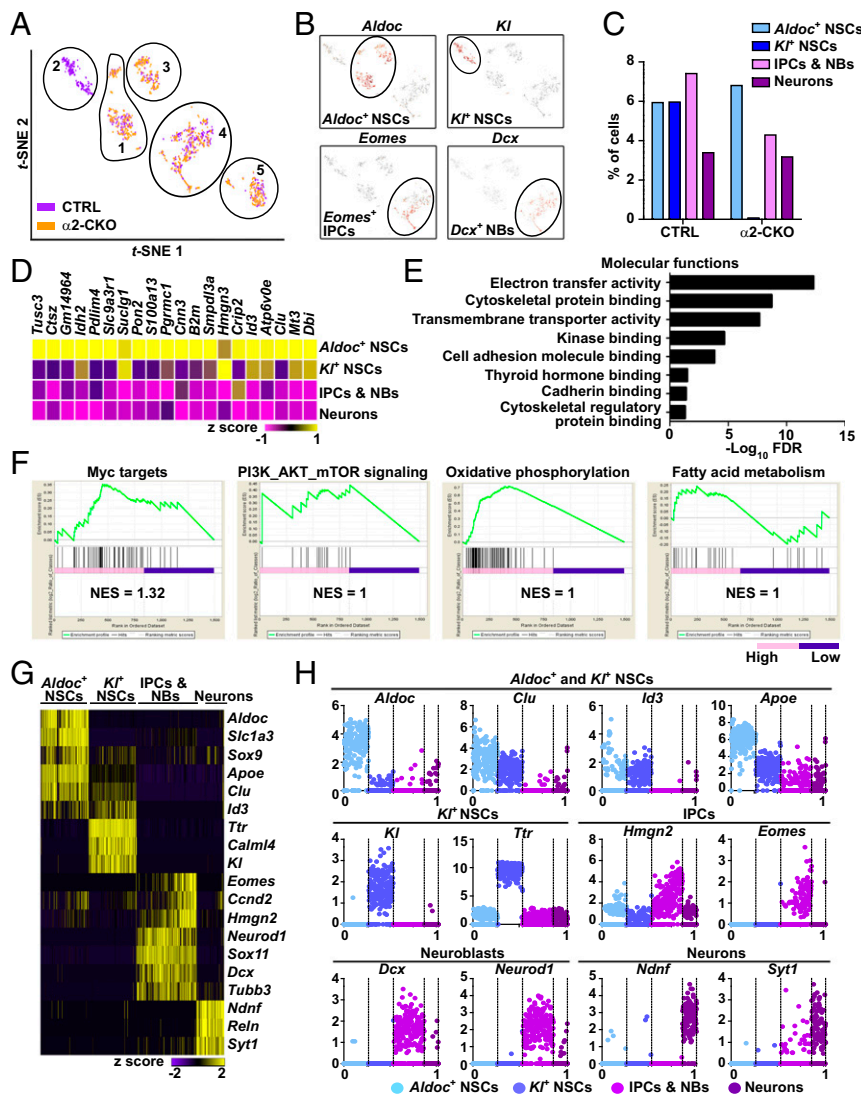To further demonstrate the switching of the NSCs/NPCs division mode in the α2-CKO mice, we lineage traced individual

**Fig. 4.** Absence of a specific *Kl*[+] NSC subpopulation from the DG niche in adult α2-CKO mice. (*A*) Zoomed-in *t*-SNE plot of NSCs (C1–C3), IPCs and NBs (C4), and neurons (C5) in CTRL and α2-CKO mice (CTRL: *n* = 822 cells, purple dots; α2-CKO: *n* = 809 cells, yellow dots). Note that C2 was found in CTRL mice but not in α2-CKO mice. (*B*) *t*-SNE plots showing *Aldoc* expression in C1 and C3 (*Aldoc*[+] NSCs), *Kl* expression in C2 (*Kl*[+] NSCs), and *Eomes*-expressing IPCs and *Dcx*-expressing NBs in C4. (*C*) Quantification of the percentage of *Aldoc*[+] NSCs, *Kl*[+] NSCs, IPCs and NBs, and neurons among all cells isolated from CTRL and α2-CKO mice. (*D*) Heatmap of the top 20 enriched genes in different neuronal lineage subpopulations from the genes in group 2 (G2) in K-means clustering analysis (*SI Appendix*, Fig. S3*B*). The color gradient is based on SDs, from −1.0 to 1.0. (*E*) GO analysis of the molecular functions of all significantly up-regulated genes in the *Kl*[+] NSCs compared with the other cell subpopulations. (*F*) GSEA comparing *Kl*[+] NSCs (C2) to *Aldoc*[+] NSC clusters (C1 and C3), showing the gene sets that are up-regulated in *Kl*[+] NSCs as arranged by normalized enrichment score (NES) from high to low. (*G*) Heatmap expression of a subset of neuronal lineage marker genes that are significantly enriched in each cell subpopulation. Each column represents a cell, and each row represents a gene. The color gradient is based on SDs from −2.0 to 2.0. (*H*) Expression profiles of representative genes in pseudotime analysis: transition from NSCs (i.e., *Aldoc*, *Clu*, *Id3*, and *Apoe*) to the proliferation and differentiation of neuronal progenitors (i.e., *Hmgn2*, *Eomes*, *Dcx*, and *Neurod1*) into mature neurons (i.e., *Ndnf* and *Syt1*). Note that *Kl*[+] NSCs represent an intermediate stage between *Aldoc*[+] NSCs and IPCs. Gene expression is shown as normalized transcript counts on the *y* axis, and the *x* axis represents pseudotime normalized within [0–1]. Each dot represents one cell.

NSCs/NPCs over the long term and tracked their asymmetric and symmetric divisions in the transgenic mice by performing an in vivo clonal analysis assay (34) (Fig. 5*L*). We found that long-term TAM injection into the α2-CKO mice significantly reduced (by 73%) the percentage of cell clones generated from the asymmetric self-renewal of NSCs/NPCs, which included one NSC/NPC (labeled "R") and another cell—either an IPC or an astroglia (labeled "X") (30 dpi; Fig. 5 *L* and *N*, labeled "R+X"). In contrast, the α2-CKO mice exhibited a significantly higher (40% higher) proportion of cell clones generated by the symmetric division of NSCs/NPCs (i.e., devoid of NSCs/NPCs; Fig. 5 *L* and *N*, labeled "No R"). Thus, both short- and long-term cell

fate analyses demonstrated that loss of α2-chimaerin prematurely activates NSCs and disturbs the balance between asymmetric and symmetric division, which results in the premature differentiation of NSCs into IPCs.

**Deletion of α2-Chimaerin in Adult NSCs Leads to Phenotypic and Functional Alterations in the Hippocampus.** Our in vivo lineage tracing data demonstrated that ablation of α2-chimaerin not only reduces early adult neurogenesis but also perturbs final neuron generation in the DG in the long term (Fig. 2 *G* and *I*). Therefore, we examined the dendritic development and functional consequences of adult-born neurons lacking α2-chimaerin, including
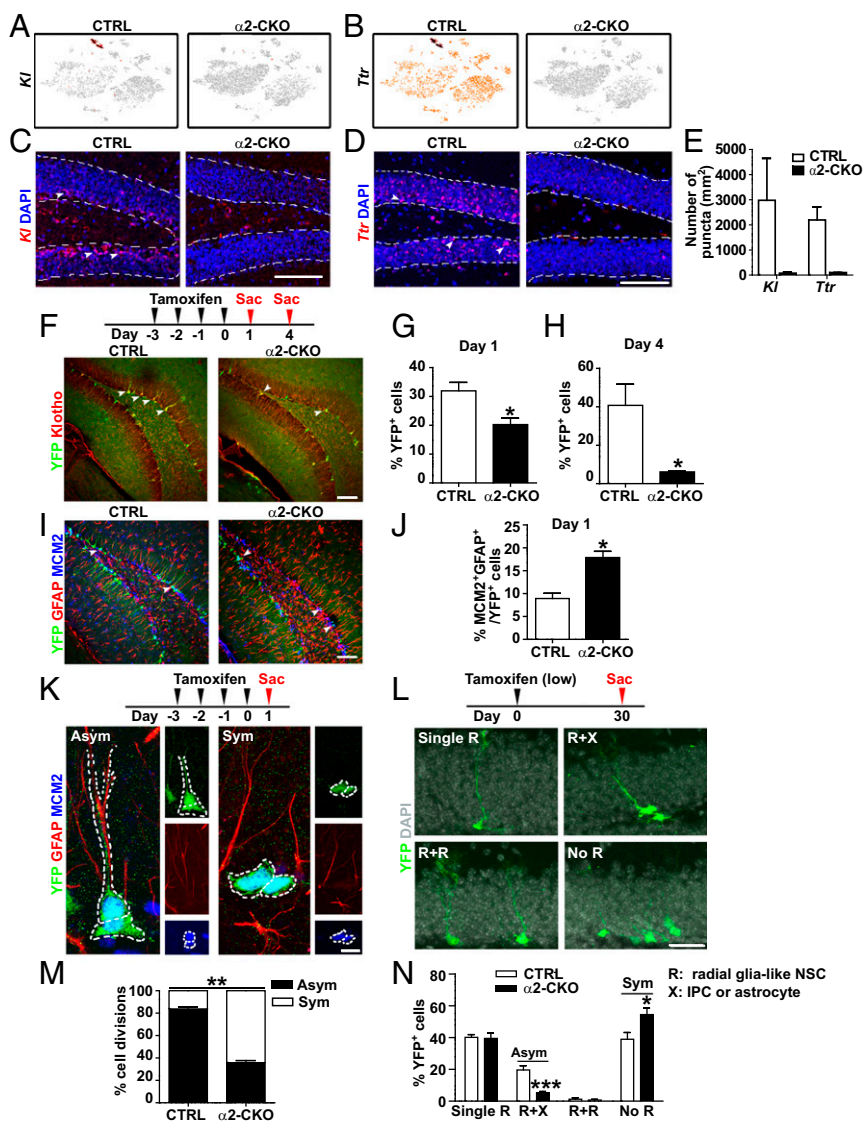
**Fig. 5.** Knockout of α2-chimaerin in adult NSCs leads to the precocious differentiation of NSCs and alters their division mode. (*A* and *B*) *t*-SNE plots showing the expressions of *Kl* (*A*) and *Ttr* (*B*) in CTRL and α2-CKO mice. (*C–E*) FISH showing the cellular expression of *Kl* transcript (*C*) and *Ttr* transcript (*D*), and their quantifications (*E*) in the hippocampal sections in CTRL and α2-CKO mice. Arrowheads indicate cells expressing *Kl* or *Ttr* transcripts. Dashed lines illustrate the contour of the granule layer in the DG. (Scale bar: 100 μm.) (*F–H*) Lineage tracing of *Kl*[+] NSCs by immunostaining of Klotho, the protein encoded by *Kl* transcript, in the DG in CTRL and α2-CKO mice. (*F*) Experimental paradigm (*Upper*), confocal images (*Lower*), and quantification (*G* and *H*) of the percentage of Klotho[+]YFP^{+} cells in the DG in CTRL and α2-CKO mice at 1 dpi (*G*) and 4 dpi (*H*). Arrowheads indicate Klotho[+]YFP^{+} cells. Values are mean ± SEM (*$P < 0.05$; 1 dpi: $n = 4$ per group; 4 dpi: CTRL: $n = 3$, α2-CKO: $n = 4$ per group; unpaired two-tailed *t* test). (Scale bar: 75 μm.) (*I* and *J*) Labeling of activated NSCs/NPCs in the DG in CTRL and α2-CKO mice. Confocal images (*I*) and quantification (*J*) of the percentage of activated NSCs/NPCs (MCM2^{+}GFAP[+]YFP^{+} cells) among YFP^{+} cells in the DG in CTRL and α2-CKO mice at 1 dpi. Arrowheads indicate the labeled MCM2^{+}GFAP[+]YFP^{+} cells. Values are mean ± SEM ($n = 3$ per group; *$P < 0.05$; unpaired two-tailed *t* test). (Scale bar: 75 μm.) (*K–N*) Visualization of the asymmetric and symmetric division of NSCs/NPCs in the DG in CTRL and α2-CKO mice. (*K*) Experimental paradigm (*Upper*), representative images in CTRL mice (*Lower*), and quantification (*M*) of asymmetric (*Left*) and symmetric (*Right*) division of adult NSCs/NPCs at 1 dpi. Actively dividing cells were labeled with MCM2. Values are mean ± SEM ($n = 3$ per group; **$P < 0.01$; unpaired two-tailed *t* test). (Scale bar: 15 μm.) (*L*) Schematic diagram of TAM administration (low dosage: 62 mg·kg^{−1}·day^{−1} i.p., *Upper*) and representative images (*Lower*) showing different modes of NSC division in clonal analysis in CTRL mice at 30 dpi. The clones show quiescent NSCs (*Upper Left*: "R," a radial glia-like NSC), asymmetrically differentiated NSCs (*Upper Right*: "R+X," where X is an IPC or astrocyte), expanded NSCs (*Lower Left*: "R+R"), and symmetrically differentiated NSCs (*Lower Right*: "No R"). (Scale bar: 30 μm.) (*N*) Frequencies of different types of NSC division among all clones in CTRL and α2-CKO mice. Values are mean ± SEM (CTRL: $n = 5$, α2-CKO: $n = 6$ per group; R+X: ***$P < 0.001$; No R: *$P < 0.05$; unpaired two-tailed *t* test).

dendritic arbors and the integration of neurons into existing circuitry. We analyzed the YFP^{+} cells in the α2-CKO mice at 30 dpi, because the dendritic morphology of adult-born neurons beyond 4 wk old is reported to be similar to that of 8-wk-old neurons (2). Compared with the CTRL mice, the newborn neurons in the α2-CKO mice exhibited reduced dendritic arborization (Fig. 6 *A* and *B*) and shorter total dendrite length (Fig. 6*C*), suggesting impaired

dendritic development. Knockdown of α2-chimaerin significantly decreased the dynamics, branching, and total length of neurites in cultured adult-born neurons derived from adult SGZ NSCs/NPCs (*SI Appendix*, Fig. S6 *A–G*). In addition, we labeled the proliferating progenitors and their progenies in the α2-KO mice by injecting GFP-expressing retrovirus into the DG. Accordingly, ablation of α2-chimaerin led to a similar decrease in total dendrite
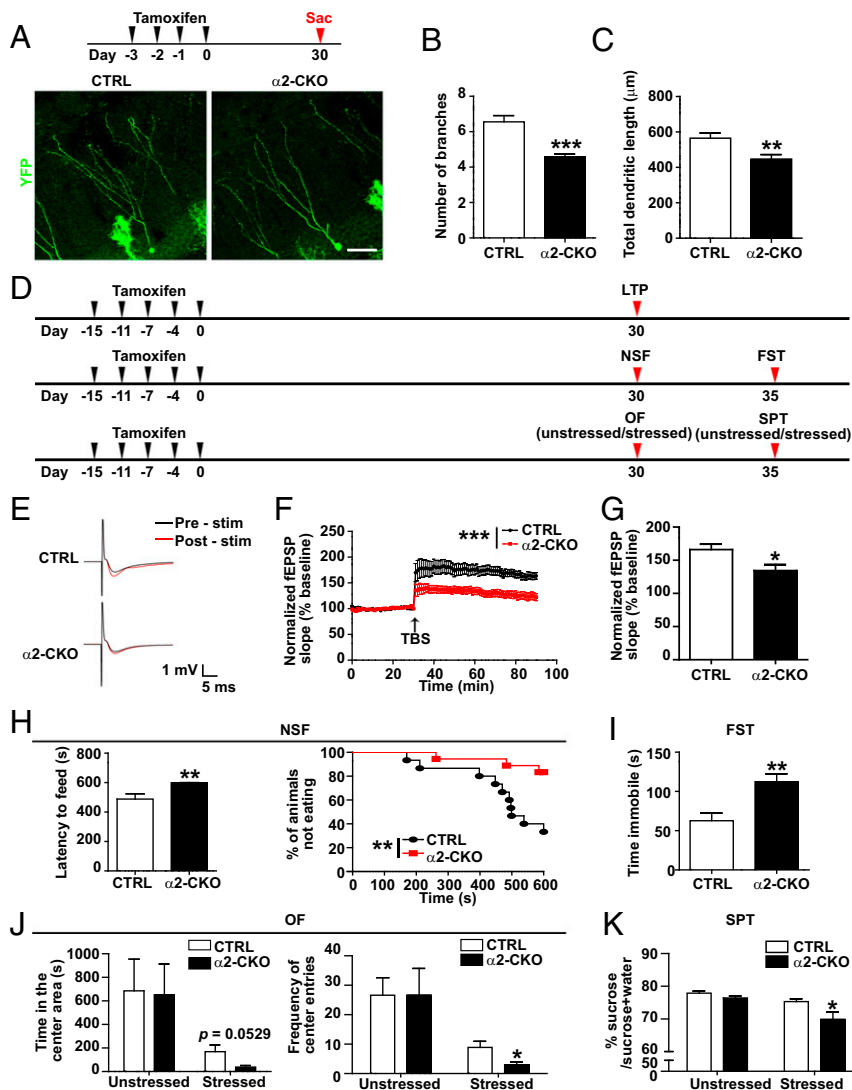
**Fig. 6.** α2-CKO mice exhibit simplified dendritic arbors in adult-born hippocampal neurons and anxiety/depression-like behaviors. (*A–C*) Dendritic morphology of adult-born hippocampal neurons in α2-CKO mice. (*A*) Experimental paradigm (*Upper*) and representative images (*Lower*) of YFP⁺ adult-born hippocampal neurons in the DG in CTRL and α2-CKO mice at 30 dpi. (Scale bar: 45 μm.) (*B* and *C*) Quantification of dendrites (*B*) and total dendritic length (*C*) of YFP⁺ neurons. Values are mean ± SEM (CTRL: $n = 34$ neurons; α2-CKO: $n = 31$ neurons from six mice per group; number of branches: ***$P < 0.001$; total dendritic length: **$P < 0.01$; unpaired two-tailed *t* test). (*D*) Schematic diagram illustrating the timeline of TAM administration, LTP, and anxiety/depression-like behavior tests. (*E–G*) Decrease of LTP in the medial perforant path in α2-CKO mice. LTP was induced by TBS. (*E*) Traces are representative field excitatory postsynaptic potentials (fEPSPs) recorded before (black) and after (red) TBS in CTRL and α2-CKO mice. (*F*) LTP as assessed by measuring the fEPSP slope (percentage of baseline) in CTRL and α2-CKO mice. (*G*) Magnitude of LTP assessed by fEPSP slope (percentage of baseline) in the last 10 min within 60 min after TBS in CTRL and α2-CKO mice. Values are mean ± SEM (CTRL: $n = 14$ slices, α2-CKO: $n = 11$ slices from six mice per group; ***$P < 0.001$; unpaired two-tailed *t* test). (*H–K*) α2-CKO mice exhibit anxiety/depression-like behaviors as indicated by the NSF test (*H*), FST (*I*), OF test (*J*), and the SPT (*K*). (*H*) Feeding latency (*Left*) and cumulative curve of the percentages of CTRL and α2-CKO mice that did not eat over a 10-min period (*Right*) ($n = 15$ per group; **$P < 0.01$; Mantel–Cox log-rank test) in the NSF test. Values are mean ± SEM (latency to feed: $n = 15$ per group; **$P < 0.01$; unpaired two-tailed *t* test). (*I*) Immobility time of CTRL and α2-CKO mice in the FST. Values are mean ± SEM (CTRL: $n = 15$; α2-CKO: $n = 14$ per group; **$P < 0.01$; unpaired two-tailed *t* test). (*J*) Time CTRL and α2-CKO mice spent in the center arena (*Left*) and total entries into the center area (*Right*) with or without 30 min of restraint stress in the OF test. Values are mean ± SEM (CTRL: $n = 8$, α2-CKO: $n = 7$ per group; time in the center area: unstressed: $P = 0.9285$; stressed: $P = 0.0529$; frequency of center entries: unstressed: $P = 0.9934$; stressed: *$P < 0.05$; unpaired two-tailed *t* test). (*K*) Quantification of sucrose preference of CTRL and α2-CKO mice with or without 30 min of restraint stress in the SPT. Values are mean ± SEM ($n = 8$ per group; unstressed: $P = 0.1038$; stressed: *$P < 0.05$; unpaired two-tailed *t* test).

length and branching in the DG (*SI Appendix*, Fig. S6 *H–J*). Therefore, deletion of α2-chimaerin leads to impaired dendritic development in adult-born neurons.

The development of dendrites on newborn neurons in the DG is critical for their integration into brain circuitry, which contributes to the potentiation of synaptic plasticity, especially in the entorhinal cortex–DG circuitry (35, 36). Therefore, we examined whether deletion of α2-chimaerin impairs the integration of newborn neurons and reduces synaptic plasticity in the DG.

Accordingly, we measured the long-term potentiation (LTP) of the afferent medial perforant pathways, which is believed to be dependent on adult neurogenesis (35), in the α2-CKO mice at 30 dpi, when newborn neurons should integrate into the neuronal circuitry (Fig. 6*D*). While LTP was induced in both groups, LTP was lower in the α2-CKO mice than the CTRL mice (Fig. 6 *E–G*), suggesting that the impaired neurogenesis induced by α2-chimaerin deletion perturbs the circuitry integration of newborn neurons and attenuates synaptic plasticity in the DG.

Given that impaired adult hippocampal neurogenesis is implicated in anxiety/depression-like behaviors, we examined whether the α2-CKO mice had altered anxiety/depression behavioral performance (Fig. 6D). The locomotor activity of the CTRL and α2-CKO mice was comparable in the open field test (*SI Appendix*, Fig. S6K). However, the α2-CKO mice exhibited significantly longer latency to start feeding in the novelty-suppressed feeding test (NSF) than the CTRL mice (Fig. 6H), indicating that they had higher anxiety/depression levels. Meanwhile, there was no significant difference in home cage food consumption between the CTRL and α2-CKO mice (*SI Appendix*, Fig. S6L), which excludes the possibility that the results were due to a difference in appetite between these two mouse lines. Similarly, the α2-CKO mice had significantly longer periods of immobility in the forced swim test (FST), indicating higher levels of anxiety/depression in this learned helplessness model of depression (Fig. 6I).

Adult neurogenesis is reported to be integral for stress resilience/susceptibility and essential for buffering stress-induced, anxiety/depression-like behaviors (8, 37). Therefore, the elevated affective behaviors observed in the α2-CKO mice during the novelty-suppressed feeding and forced swim tests could reflect their impaired ability to overcome stress. To determine whether α2-chimaerin ablation in adults NSCs alters the stress response of mice, we introduced the mice to a moderate restraint stressor before subjecting them to the open field test (OF) or sucrose preference test (SPT) (Fig. 6D) (37). Under the unstressed condition, we observed no obvious differences between the CTRL and α2-CKO mice in either test (Fig. 6 J and K). However, the α2-CKO mice showed significantly higher levels of anxiety/depression after they were subjected to a moderate restraint stressor. Specifically, α2-CKO mice subjected to restraint spent dramatically less time in the center zone, had fewer center entries in the open field test (Fig. 6J; showing highly anxious performance), and consumed less sucrose in the sucrose preference test (Fig. 6K). Because the total amount of sucrose consumed was comparable between the CTRL and α2-CKO mice, the preference of the α2-CKO mice was not due to the motivation to drink (*SI Appendix*, Fig. S6M). Therefore, these results collectively demonstrate that conditional deletion of α2-chimaerin in adult hippocampal NSCs leads to elevated anxiety/depression levels in mice, especially in response to stress.

## Discussion

A remarkable feature of NSCs in adult neurogenesis is that they constantly maintain homeostasis to ensure continuous neuron generation while preserving a sufficient NSC pool. Disrupting NSC homeostasis results in uncontrolled cell expansion or premature NSC depletion, which leads to abnormally elevated or decreased neurogenesis. Nevertheless, how adult NSCs "decide" between self-renewal and differentiation in response to intrinsic or extrinsic stimuli remains poorly understood. In this study, we showed that α2-chimaerin is critical for adult NSC homeostasis in adult neurogenesis. Accordingly, loss of α2-chimaerin in adult NSCs resulted in the premature differentiation of NSCs, which led to the depletion of the NSC pool. In the long term, loss of α2-chimaerin led to decreased neurogenesis, compromised synaptic plasticity, and impaired hippocampal function, which resembles the hallmarks of adult neurogenesis defects during aging.

Characterizing the temporal development of adult hippocampal NSCs advances our understanding of adult neurogenesis, which has been made difficult owing to their heterogeneity. The recent advance in extensive profiling of this cellular diversity within the adult DG neurogenic niche using scRNA-seq analysis has contributed to resolving this challenge (9, 38). The progression of NSCs is characterized by a continuum of molecular and cellular events: quiescent NSCs prepare for cellular differentiation by accelerating protein/RNA biogenesis, mobilizing cell cycle-related genes, and switching from glycolysis-dependent metabolism to both oxidative phosphorylation and fatty acid metabolism (9, 33, 39, 40). These cellular pathways provide molecular candidates for the study of the cell fate controls of different NSC subpopulations. Combining scRNA-seq with lineage tracing approaches to understand the roles of α2-chimaerin in adult hippocampal NSCs enables us to examine the heterogeneity of adult NSCs in high resolution and probe the differential lineage progression of specific NSC subpopulations. Accordingly, this combined approach revealed that the Nestin-driven α2-CKO mice lacked a $Kl^+$ NSC subpopulation that represents a critical cell-stage transition from NSCs to IPCs. This $Kl^+$ NSC subpopulation is associated with the expression of components of pathways, including Myc targets, PI3K_AKT_mTOR, oxidative phosphorylation, and fatty acid metabolism pathways (Fig. 4 and *SI Appendix*, Fig. S4). These pathways are part of a highly active metabolic program that is vital for supplying energy for NSC activation and their subsequent differentiation (18).

Identifying distinct NSC subpopulations helps resolve the process of adult neurogenesis. To our knowledge, the $Kl^+$ NSC subpopulation herein has not been previously reported. This subpopulation has a unique signature, namely high expression of Klotho and Ttr (Fig. 4 and *SI Appendix*, Fig. S5). Interestingly, Klotho-knockout mice exhibit decreased proliferation of adult NSCs/NPCs and impaired maturation of young neurons in the DG, whereas Klotho overexpression in adult mice increases the NSC pool and the number of immature neurons with enhanced dendritic branches (26). The restrictive expression of Klotho in $Kl^+$ NSCs in the hippocampus suggests that this NSC subpopulation may serve as a niche to provide signals to regulate the proliferation of NSCs. Since a decrease in the hippocampal NSC pool is one of the obvious signs of aging or related diseases, it would be interesting to examine whether deregulation of the $Kl^+$ NSC subpopulation mediates the loss of the NSC pool. Meanwhile, Ttr is a transport protein of the thyroid hormone and retinol that regulates the differentiation capacity of neurospheres derived from the adult subventricular zone (41). Hence, it would be of interest to further examine the roles of the $Kl^+$ NSC subpopulation and Klotho and Ttr in the regulation of adult NSC proliferation and differentiation.

During adult neurogenesis, extrinsic cues transduce signals that trigger downstream intracellular pathways, which dictate the fate of NSCs and the tempo of this developmental process (12). Activation of the signal protein, α2-chimaerin, can transduce signals from cell surface receptors to intracellular effectors; therefore, future studies are warranted to determine how α2-chimaerin integrates the extrinsic signals during adult neurogenesis. Given that α2-chimaerin is a negative regulator of Rac1 and various lineage tracing studies suggest that Rac1 regulates adult NSC/NPC proliferation as well as the dendrite development of adult-born neurons in adult neurogenesis (22, 23, 42, 43), it is of interest to examine whether α2-chimaerin integrates extracellular neurogenic signals, such as neurotrophins and neurotransmitters, through Rac1 during adult neurogenesis. For example, GABAergic inputs from proximal parvalbumin-expressing interneurons are critical for deciding between NSC quiescence and activation via GABA$_A$ receptor expressed in adult hippocampal NSCs (44), and Rac1 activity is required to maintain full GABA$_A$ receptor activity (45). Therefore, we speculate that α2-chimaerin regulates the fate decision of adult NSCs through Rac1 activity downstream of GABA signaling.

In summary, our findings reveal the role of α2-chimaerin in adult hippocampal neurogenesis. We demonstrated that specific deletion of α2-chimaerin induces the premature differentiation of NSCs, impairs the generation and maturation of adult-born hippocampal neurons, and affects normal brain functions. Given that adult neurogenesis is an important regulator of anxiety and depression, our findings advance the understanding of adult

NEUROSCIENCE

NSCs and provide insights into the molecular mechanisms that underlie anxiety and depression.

## Materials and Methods

**Animals and Drug Administration.** All mice were housed at the Hong Kong University of Science and Technology (HKUST) Animal and Plant Care Facility, and the HKUST Animal Ethics Committee approved all animal experiments. For details of mice generation and drug administration, see *SI Appendix, Methods*.

**Immunohistochemistry and FISH.** We used antibodies of α2-chimaerin, Tbr2, DCX, Nestin, BrdU, GFAP, Ki67, NeuN, active caspase-3, GFP, Ttr, Klotho, and MCM2 for immunostaining. For details, see *SI Appendix, Methods*.

The templates for the synthesis of riboprobes for *Ttr* and *Kl* were full-length *Ttr* cDNA and the 810 bp of the N-terminal of *Kl* cDNA, respectively (46). For details, see *SI Appendix, Methods*.

**The 10× Genomics scRNA-Seq and Pathway Analysis.** We performed scRNA-seq according to the manufacturer's protocol (10× Chromium Single Cell 3′ Reagent Kit, version 2; 10× Genomics). Details for the pseudotime analysis, GO analysis, STRING analysis, and GSEA analysis are provided in *SI Appendix, Methods*.

**Virus Injection, Electrophysiology, and Behavioral Tests.** GFP-expressing retroviruses were bilaterally injected into the DG of WT and α2-KO mice, and brain sections were analyzed at 30 dpi. For details, see *SI Appendix, Methods*.

LTP was induced at the afferents of the medial perforant pathways, and measurement was set at the molecular layer of the DG using theta-burst stimulation (TBS). We measured the magnitude of LTP for 60 min after TBS (*SI Appendix, Methods*).

All behavioral tests were carried out on mice 3–4 wk after TAM injection starting from 2 to 3 mo of age (Fig. 6*D*). For details of each behavioral experiment, see *SI Appendix, Methods*.

**Quantification and Statistical Analyses.** Details for quantification and statistical analyses can be found in *SI Appendix, Methods*.

1. J. T. Gonçalves, S. T. Schafer, F. H. Gage, Adult neurogenesis in the hippocampus: From stem cells to behavior. *Cell* **167**, 897–914 (2016).
2. C. Zhao, E. M. Teng, R. G. Summers, Jr, G. L. Ming, F. H. Gage, Distinct morphological stages of dentate granule neuron maturation in the adult mouse hippocampus. *J. Neurosci.* **26**, 3–11 (2006).
3. D. X. Yu, M. C. Marchetto, F. H. Gage, How to make a hippocampal dentate gyrus granule neuron. *Development* **141**, 2366–2375 (2014).
4. A. M. Bond, G. L. Ming, H. Song, Adult mammalian neural stem cells and neurogenesis: Five decades later. *Cell Stem Cell* **17**, 385–395 (2015).
5. H. Mira et al., Signaling through BMPR-IA regulates quiescence and long-term activity of neural stem cells in the adult hippocampus. *Cell Stem Cell* **7**, 78–89 (2010).
6. K. T. Gobeske et al., BMP signaling mediates effects of exercise on hippocampal neurogenesis and cognition in mice. *PLoS One* **4**, e7506 (2009).
7. O. Ehm et al., RBPJkappa-dependent signaling is essential for long-term maintenance of neural stem cells in the adult hippocampus. *J. Neurosci.* **30**, 13794–13807 (2010).
8. C. Anacker, R. Hen, Adult hippocampal neurogenesis and cognitive flexibility–Linking memory and mood. *Nat. Rev. Neurosci.* **18**, 335–346 (2017).
9. J. Shin et al., Single-cell RNA-seq with waterfall reveals molecular cascades underlying adult neurogenesis. *Cell Stem Cell* **17**, 360–372 (2015).
10. H. Hochgerner, A. Zeisel, P. Lönnerberg, S. Linnarsson, Conserved properties of dentate gyrus neurogenesis across postnatal development revealed by single-cell RNA sequencing. *Nat. Neurosci.* **21**, 290–299 (2018).
11. B. W. Dulken, D. S. Leeman, S. C. Boutet, K. Hebestreit, A. Brunet, Single-cell transcriptomic analysis defines heterogeneity and transcriptional dynamics in the adult neural stem cell lineage. *Cell Rep.* **18**, 777–790 (2017).
12. G. L. Ming, H. Song, Adult neurogenesis in the mammalian brain: Significant answers and significant questions. *Neuron* **70**, 687–702 (2011).
13. A. Sierra et al., Microglia shape adult hippocampal neurogenesis through apoptosis-coupled phagocytosis. *Cell Stem Cell* **7**, 483–495 (2010).
14. R. Faigle, H. Song, Signaling mechanisms regulating adult neural stem cells and neurogenesis. *Biochim. Biophys. Acta* **1830**, 2435–2448 (2013).
15. T. D. Palmer, A. R. Willhoite, F. H. Gage, Vascular niche for adult hippocampal neurogenesis. *J. Comp. Neurol.* **425**, 479–494 (2000).
16. J. Andersen et al., A transcriptional mechanism integrating inputs from extracellular signals to activate hippocampal stem cells. *Neuron* **83**, 1085–1097 (2014).
17. J. Jin et al., miR-17-92 cluster regulates adult hippocampal neurogenesis, anxiety, and depression. *Cell Rep.* **16**, 1653–1663 (2016).
18. K. Ito, K. Ito, Metabolism and the control of cell fate decisions and stem cell renewal. *Annu. Rev. Cell Dev. Biol.* **32**, 399–409 (2016).
19. L. Van Aelst, C. D'Souza-Schorey, Rho GTPases and signaling networks. *Genes Dev.* **11**, 2295–2322 (1997).
20. S. Etienne-Manneville, A. Hall, Rho GTPases in cell biology. *Nature* **420**, 629–635 (2002).
21. E.-E. Govek, S. E. Newey, L. Van Aelst, The role of the Rho GTPases in neuronal development. *Genes Dev.* **19**, 1–49 (2005).
22. D. P. Leone, K. Srinivasan, C. Brakebusch, S. K. McConnell, The rho GTPase Rac1 is required for proliferation and survival of progenitors in the developing forebrain. *Dev. Neurobiol.* **70**, 659–678 (2010).
23. K. C. Vadodaria, C. Brakebusch, U. Suter, S. Jessberger, Stage-specific functions of the small Rho GTPases Cdc42 and Rac1 for adult hippocampal neurogenesis. *J. Neurosci.* **33**, 1179–1189 (2013).
24. T. R. Stankiewicz, D. A. Linseman, Rho family GTPases: Key players in neuronal development, neuronal survival, and neurodegeneration. *Front. Cell. Neurosci.* **8**, 314 (2014).
25. A. Zeisel et al., Molecular architecture of the mouse nervous system. *Cell* **174**, 999–1014.e22 (2018).
26. A. M. Laszczyk et al., Klotho regulates postnatal neurogenesis and protects against age-related spatial memory loss. *Neurobiol. Aging* **59**, 41–54 (2017).
27. H. Liu et al., Augmented Wnt signaling in a mammalian model of accelerated aging. *Science* **317**, 803–806 (2007).
28. I. Dumitru, A. Neitz, J. Alfonso, H. Monyer, Diazepam binding inhibitor promotes stem cell expansion controlling environment-dependent neurogenesis. *Neuron* **94**, 125–137.e5 (2017).
29. S. A. Yuzwa et al., Developmental emergence of adult neural stem cells as revealed by single-cell transcriptional profiling. *Cell Rep.* **21**, 3970–3986 (2017).
30. C. Bohrer et al., The balance of Id3 and E47 determines neural stem/precursor cell differentiation into astrocytes. *EMBO J.* **34**, 2804–2819 (2015).
31. R. Cao et al., Quantitative proteomic analysis of membrane proteins involved in astroglial differentiation of neural stem cells by SILAC labeling coupled with LC-MS/MS. *J. Proteome Res.* **11**, 829–838 (2012).
32. V. Cavallucci, M. Fidaleo, G. Pani, Neural stem cells and nutrients: Poised between quiescence and exhaustion. *Trends Endocrinol. Metab.* **27**, 756–769 (2016).
33. R. Beckervordersandforth et al., Role of mitochondrial metabolism in the control of early lineage progression and aging phenotypes in adult hippocampal neurogenesis. *Neuron* **93**, 560–573.e6 (2017).
34. M. A. Bonaguidi et al., In vivo clonal analysis reveals self-renewing and multipotent adult neural stem cell characteristics. *Cell* **145**, 1142–1155 (2011).
35. J. S. Snyder, N. Kee, J. M. Wojtowicz, Effects of adult neurogenesis on synaptic plasticity in the rat dentate gyrus. *J. Neurophysiol.* **85**, 2423–2431 (2001).
36. A. Marín-Burgin, L. A. Mongiat, M. B. Pardi, A. F. Schinder, Unique processing during a period of high excitation/inhibition balance in adult-born neurons. *Science* **335**, 1238–1242 (2012).
37. J. S. Snyder, A. Soumier, M. Brewer, J. Pickel, H. A. Cameron, Adult hippocampal neurogenesis buffers stress responses and depressive behaviour. *Nature* **476**, 458–461 (2011).
38. B. Artegiani et al., A single-cell RNA sequencing study reveals cellular and molecular dynamics of the hippocampal neurogenic niche. *Cell Rep.* **21**, 3271–3284 (2017).
39. M. Khacho et al., Mitochondrial dynamics impacts stem cell identity and fate decisions by regulating a nuclear transcriptional program. *Cell Stem Cell* **19**, 232–247 (2016).
40. M. Khacho, R. Harris, R. S. Slack, Mitochondria as central regulators of neural stem cell fate and cognitive function. *Nat. Rev. Neurosci.* **20**, 34–48 (2019).
41. R. Kapoor, S. E. Fanibunda, L. A. Desouza, S. K. Guha, V. A. Vaidya, Perspectives on thyroid hormone action in adult neurogenesis. *J. Neurochem.* **133**, 599–616 (2015).
42. U. Haditsch et al., Neuronal Rac1 is required for learning-evoked neurogenesis. *J. Neurosci.* **33**, 12229–12241 (2013).
43. X.-T. Yang et al., Rac1 guides porf-2 to Wnt pathway to mediate neural stem cell proliferation. *Front. Mol. Neurosci.* **10**, 172 (2017).
44. J. Song et al., Neuronal circuitry mechanism regulating adult quiescent neural stem-cell fate decision. *Nature* **489**, 150–154 (2012).
45. D. K. Meyer et al., Regulation of somatodendritic GABAA receptor channels in rat hippocampal neurons: Evidence for a role of the small GTPase Rac1. *J. Neurosci.* **20**, 6743–6751 (2000).
46. H. Li et al., Soluble amyloid precursor protein (APP) regulates transthyretin and Klotho gene expression without rescuing the essential function of APP. *Proc. Natl. Acad. Sci. U.S.A.* **107**, 17362–17367 (2010). Erratum in: *Proc. Natl. Acad. Sci. U.S.A.* **110**, 13228 (2013).